Spherical cluster method for ground state determination of site-disordered materials: application to $Ag_xBi_yI_{x+3y}$

Victor T. Barone[1*], Blair R. Tuttle[2], Sanjay V. Khare[1]

[1]Department of Physics, Wright Center for Photovoltaics Innovation and Commercialization, University of Toledo, Toledo, Ohio 43606, USA

[2]Department of Physics, Penn State Behrend, Erie, Pennsylvania 16563, USA

*Author to whom correspondence should be addressed: vbarone@rockets.utoledo.edu

Supplemental information for V.T. Barone et. al.

Calculation of the number of combinations for a given crystal system

Let L be the number of sublattices present in the system, and let l enumerate them.

Let E_l be the number of unique elements in sublattice l, and let e_l enumerate them.

Let S_l be the total number of sites in sublattice l.

Let S_{l,e_l} be the number of sites in sublattice l of element e_l.

$$\#\ \text{Combinations} = \prod_{l}^{L}\left[\prod_{e_l}^{E_l}\binom{S_l - \sum_{j}^{e_l-1} S_{l,j}}{S_{l,e_l}}\right]$$

The factor in parenthesis is the binomial coefficient:

$$\binom{n}{k} = \frac{n!}{k!\,(n-k)!}$$

It is more intuitive to follow an example.

Consider a $2 \times 2 \times 1$ cell of $AgBiI_4$ following the restrictions of **Table I, row 2**. There are seven total sublattices: three of *layer 1*, three of *layer 2*, and one iodine sublattice with has no site disorder (we will therefore ignore it). Each layer contains four sites.

Layer 1's site distribution is zero Ag, one Bi, and three Va. For *Layer 1*, call the factor in square brackets N_1.

$$N_1 = \binom{4}{0}\binom{4-(0)}{1}\binom{4-(0+1)}{3} = 4.$$

Layer 2's site distribution is two Ag, one Bi, and one Va. For *Layer 2*, call the factor in square brackets N_2.

$$N_2 = \binom{4}{2}\binom{4-(2)}{1}\binom{4-(2+1)}{1} = 12.$$

Then performing the product over L (ignoring the iodine sublattice, where the factor in square brackets is 1) gives

$$\#\ \text{Combinations} = N_1 N_1 N_1 N_2 N_2 N_2 = 110592$$

since there are three of each layer per cell.

Effects of Different Exchange-Correlation Functionals

Here, we list some basic properties of the minimum-energy $AgBiI_4$ cell when treated with a few different XC functionals. Mind, in the main text, we use the GGA-PBE functional. The calculation parameters for results displayed here follow the DFT section in the main text. We also attempted to use the MBJ functional, however, it was unable to converge to a solution even with a pre-converged wavefunction and charge density.

Functional	a (Å)	c (Å)	$\max[\lvert\mathbf{r}-\mathbf{r}_{\mathrm{GGA}}\rvert]$ (Å)	Band Gap (eV)
GGA-PBE	4.46	21.33	0.00 (0.00)	1.71
PBEsol	4.36	20.88	0.49 (0.05)	1.67
DFT-D3	4.42	21.14	0.25 (0.11)	1.75
SCAN	4.42	21.13	0.25 (0.08)	1.90

Table S1. Properties of $AgBiI_4$ from **Table 1**, **row 1** computed with various XC functionals. a and c are lattice parameters, $\max\,[\lvert\mathbf{r}-\mathbf{r}_{\mathrm{GGA}}\rvert]$ is the maximum deviation in the final position of any atom in a cell relaxed with some functional compared to the same atom in a cell relaxed with GGA, and the Band Gap is the minimum energy difference between the VBM (Γ for all functionals) and the CBM ($(0.429, 0.000, 0.333)$ for all functionals). Two values are given for the entries in column four: the first is as explained above, and the second (in parentheses) removes the influence of lattice size and shape, and is therefore a measure only of atomic structure.

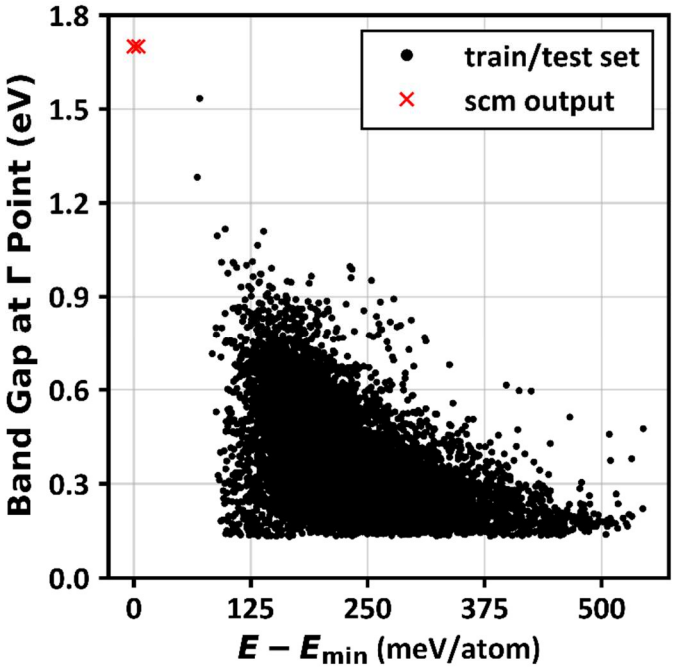

FIG. S1. Relationship between band gaps and energies of 9,202 $AgBiI_4$ models. Ignoring many body and relativistic effects, as well as the flat bands of silver bismuth-iodides, allow for reasonable estimates of the band gap with only the Γ point. The results suggest that very low-energy structures are necessary to reproduce the experimental (1.7 – 1.9 eV) band gap. The red crosses show the results of our method (SCM) in estimating the lowest energy structures. The two SCM outputs are nearly overlapping. The SCM was trained on 460 random data points from the 9200 points shown in the train/test set.

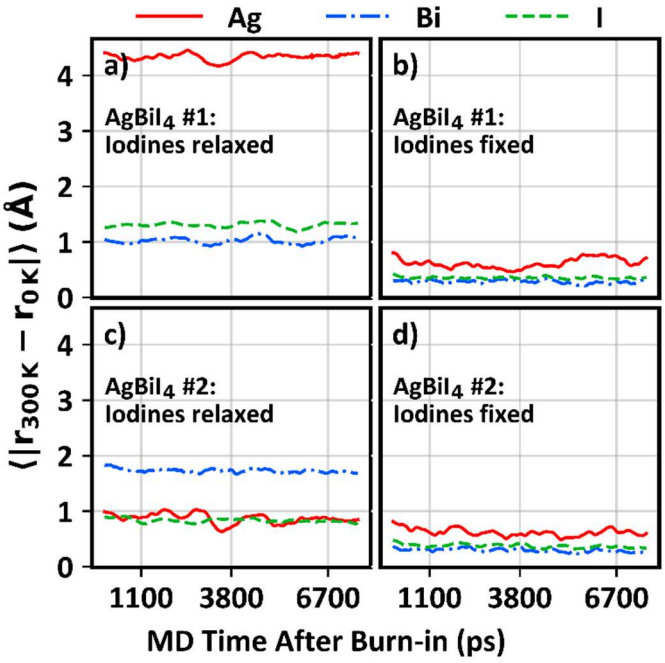

FIG. S2. Average distances between final atom positions ($\mathbf{r}_{0\ K}$) and corresponding molecular dynamics (MD) positions ($\mathbf{r}_{300\ K}$) for two $AgBiI_4$ cells. In all cases, the MD was performed at 300 K and iodine atoms were allowed to relax. **a)** and **c)** compare deviations in atom positions of the aforementioned MD with the final positions resulting from 0 K conjugate gradient (CG) minimizations. In **a)** and **c)**, the iodine atoms were allowed to relax during the CG minimizations. **b)** and **d)** are similar to **a)** and **c)** except the iodine atoms were fixed to their crystallographic positions. Comparing **a)** to **b)**, or **c)** to **d)**, shows that the CG relaxations with fixed iodine atoms more closely resemble the finite temperature MD than the CG relaxations with iodine atoms allowed to relax.

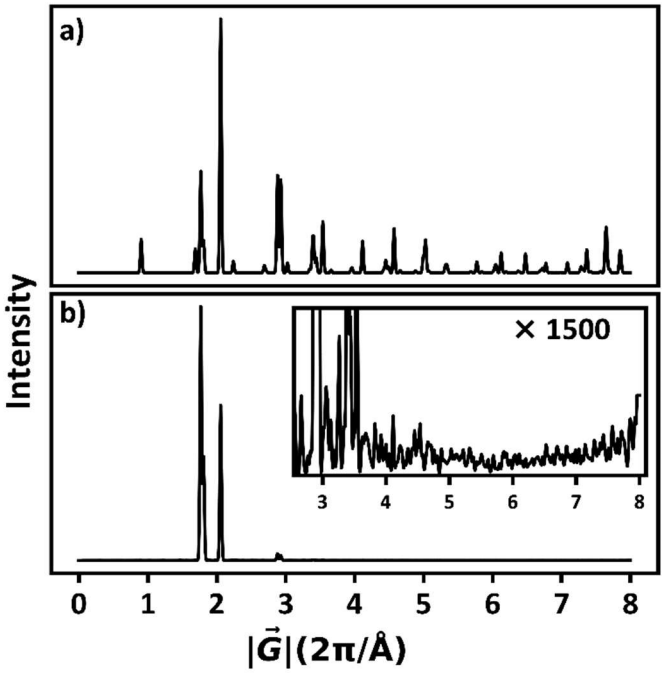

FIG. S3. a) Simulated x-ray diffraction spectra of 3000 low-energy $AgBiI_4$ models, keeping iodine fixed during relaxations. **b)** Simulated x-ray diffraction spectra of the same 3000 models as in **a)**, except all ions including iodine were allowed to relax. **(inset)** zoom-in of **b)** to show high-index signals (there are no high-index signals in **a)**). The y-axis is scaled by a factor of 1,500. Lorentz Polarization correction factors using λ = 1.5406 Å were applied in both **a)** and **b)**. **a)** compares much more favorably to experimental data [5–9] than **b)**.

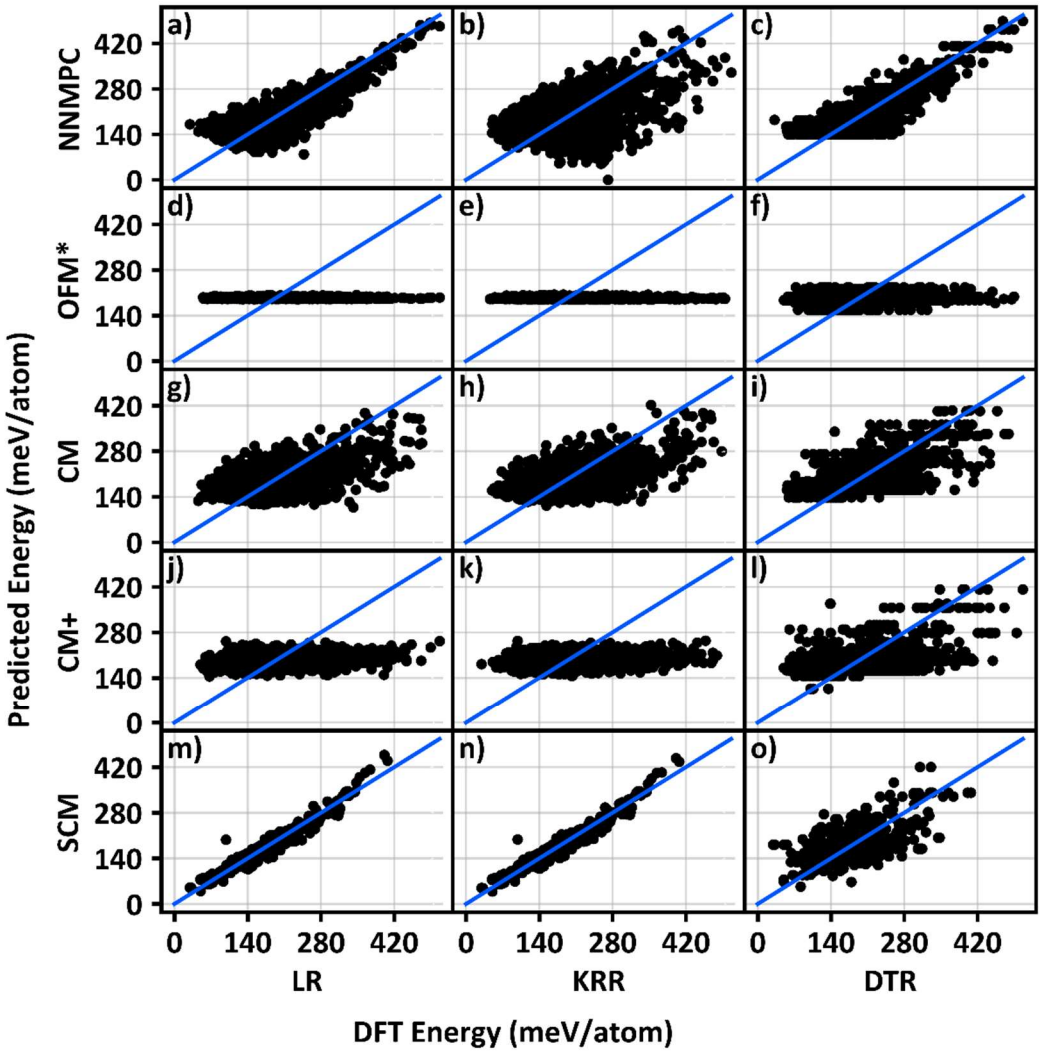

FIG. S4. Some tested energy predictions of common chemical descriptors for trigonal $AgBiI_4$. In **a-l)**, an 80-20 train-test split is applied to 9200 $AgBiI_4$ models. In **m-o)**, the spherical cluster method (SCM) was fit to 460 points. Black data points represent testing points, and the training points are not shown. The blue line is an ideal 1:1 correlation between predicted and total energies. The descriptors are organized row-wise. From top to bottom: **a-c)** nearest-neighbor metal pair counts (NNMPC) used in our previous study of cubic $AgBiI_4$ [1], **d-f)** Orbital Field Matrix (OFM) eigenspectra [2], **g-i)** Coulomb Matrix (CM) eigenspectra [3], **j-l)** a periodic-cell correction to the Coulomb Matrix (CM+) eigenspectra [4], and **m-o)** the spherical cluster method (SCM)

described in this work. Three fitting techniques are shown for each descriptor, arranged column-wise: **a, d, g, j, m)** linear regression (LR), **b, e, h, k, n)** kernel ridge regression (KRR), and **c, f, i, l, o)** decision tree regression (DTR).

*: The authors of the OFM [2] suggest using the eigenspectra of the OFM created from the average of all local contributions. Here, we instead use the average eigenspectra of each local OFM to distinguish one structure from the other. The original formulation predicts the same energy for each structure.

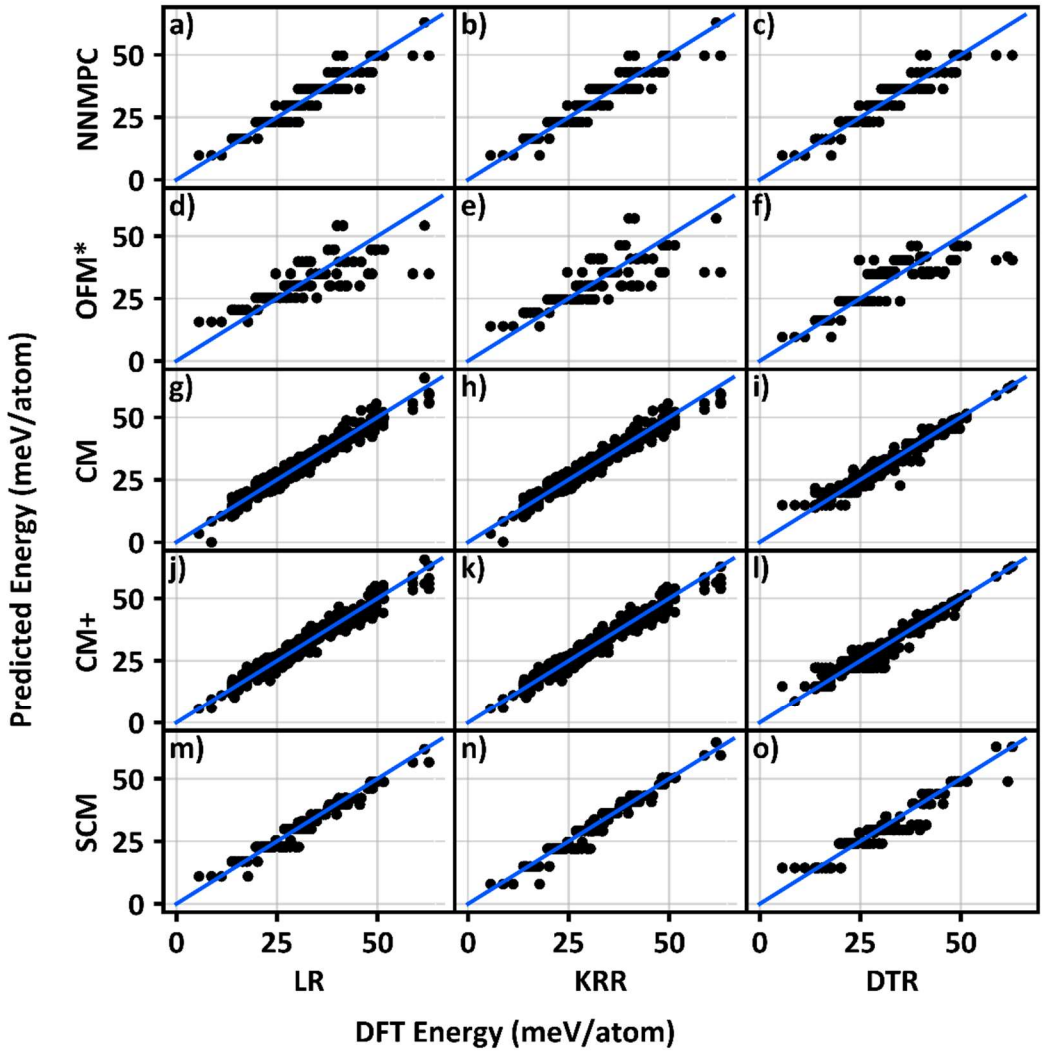

FIG. S5. Some common chemical descriptors' tested energy predictions of cubic $AgBiI_4$. In **a-l)**, an 80-20 train-test split is applied to all possible 12870 $AgBiI_4$ cells described in [1]. In **m-o)**, the spherical cluster method (SCM) was fit to 30 points. Black data points represent testing points, and the training points are not shown. The blue line is an ideal 1:1 correlation between predicted and total energies. The descriptors are organized row-wise. From top to bottom: **a-c)** nearest-neighbor metal pair counts (NNMPC) used in our previous study of cubic $AgBiI_4$ [1], **d-f)** Orbital Field Matrix (OFM) eigenspectra [2], **g-i)** Coulomb Matrix (CM) eigenspectra [3], **j-l)** a periodic-cell correction to the Coulomb Matrix (CM+) eigenspectra [4], and **m-o)** the SCM described in this work. Three fitting techniques are shown for each descriptor, arranged column-wise: **a, d, g,**

j, m) linear regression (LR), **b, e, h, k, n)** kernel ridge regression (KRR), and **c, f, i, l, o)** decision tree regression (DTR).

*: The authors of the OFM [2] suggest using the eigenspectra of the OFM created from the average of all local contributions. Here, we instead use the average eigenspectra of each local OFM to distinguish one structure from the other. The original formulation predicts the same energy for each structure.

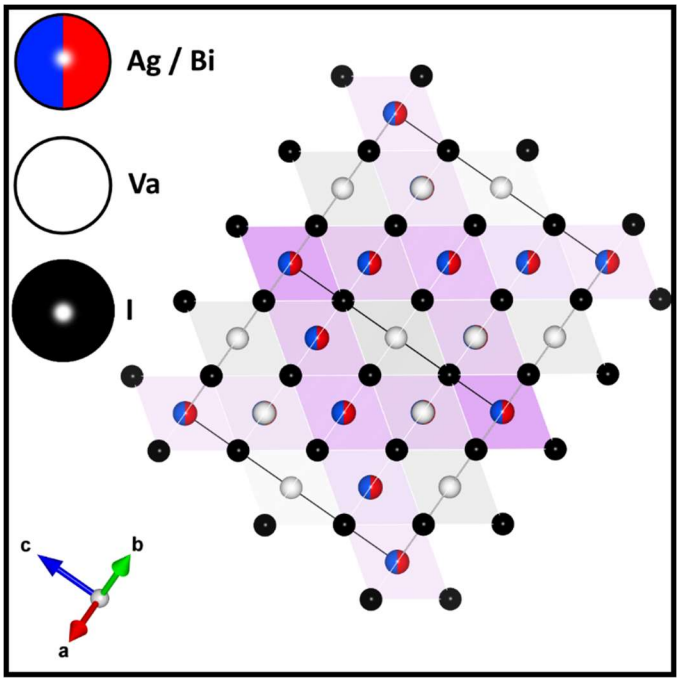

FIG. S6. The cubic unit cell of $AgBiI_4$ rotated to show its relation to the $NaVO_2$-type models. The cell contains 32 iodine sites (black dots), 16 sites whose occupancies vary between Ag and Bi (red/blue dots), and 16 sites that are fixed as vacant (white dots).

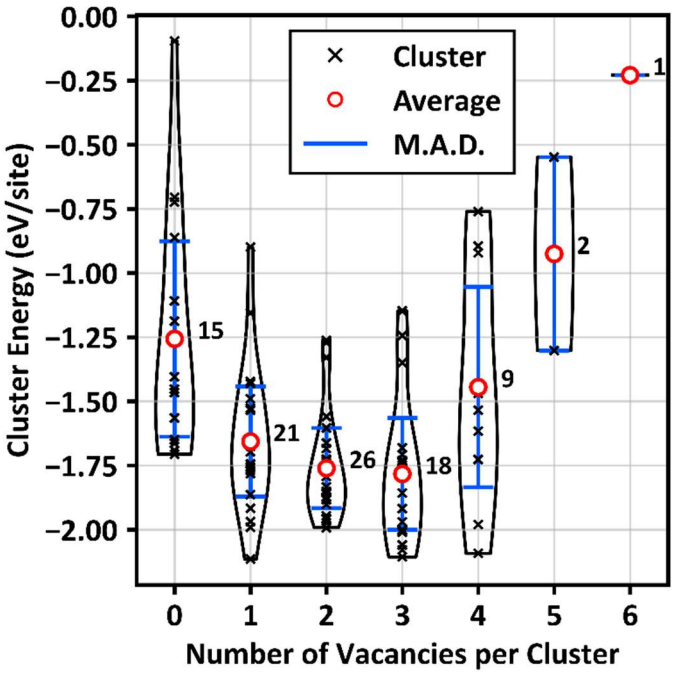

FIG. S7. Violin plot (width of black lines represent density of data points) of all 92 1st nearest neighbor (7 sites each) cluster energies vs. the number of vacant sites in each cluster. The black crosses, red circles, and blue lines represent individual data points, averages, and mean absolute deviations (M.A.D.) from the averages, respectively. The numbers to the right of each average indicate the number of data points in each group.

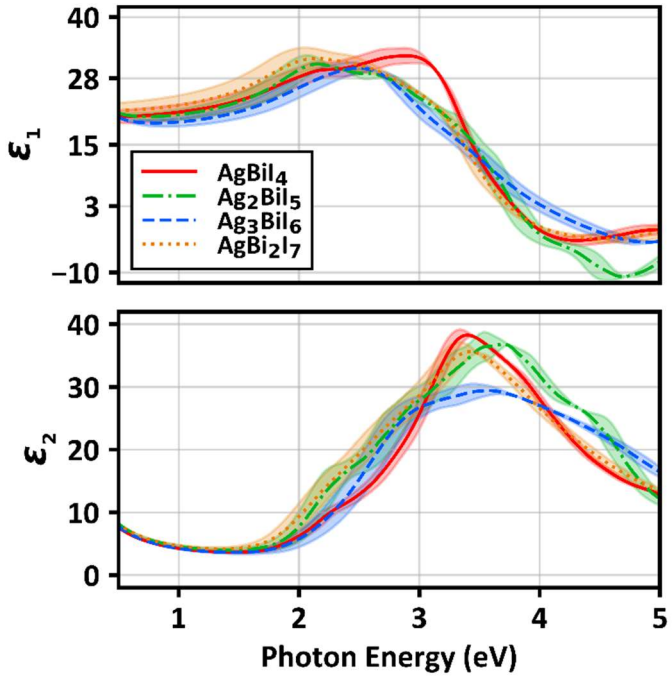

FIG. S8. PHS-corrected (PBE + HSE06 + Sum) [10] components of the complex dielectric function $\varepsilon_1 + i\varepsilon_2$ for the Ag-Bi-I cells at the first row of **Table I**. Filled regions represent deviations in the spectrum calculated with the PHS method for bandgap corrections of $\Delta E_g = \pm$ 0.1 eV (the average error between the PBE functional and the HSE06 functional with SOC interactions included). The solid lines are averages over the filled regions.

ACKNOWLEDGEMENTS

This material is based on research sponsored by the Air Force Research Laboratory under agreements No. FA9453-19-C-1002 and FA9453-21-C-0056 as well as the National Science Foundation Division of Civil, Mechanical, and Manufacturing Innovation under Grant No. 1629239. The U.S. Government is authorized to reproduce and distribute reprints for Governmental purposes notwithstanding any copyright notation thereon. The views expressed are those of the authors and do not reflect the official guidance or position of the United States Government, the Department of Defense or of the United States Air Force. The appearance of external hyperlinks does not constitute endorsement by the United States Department of Defense (DoD) of the linked websites, or the information, products, or services contained therein. The DoD does not exercise any editorial, security, or other control over the information you may find at these locations. Approved for public release; distribution is unlimited. Public Affairs release approval #AFRL-2023-1270. B.R.T. would like to acknowledge support from the National Science Foundation under Grant No. DMR-2127473.

Computations for this research were performed on the Ohio Supercomputer Center's Owens supercomputing cluster [11] and the Pennsylvania State University's Institute for Computational and Data Sciences' Roar supercomputer.

[1] V. T. Barone, B. R. Tuttle, and S. V. Khare, *Properties of $AgBiI_4$ Using High through-Put DFT and Machine Learning Methods*, Journal of Applied Physics **131**, 245701 (2022).

[2] T. Lam Pham, H. Kino, K. Terakura, T. Miyake, K. Tsuda, I. Takigawa, and H. Chi Dam, *Machine Learning Reveals Orbital Interaction in Materials*, Science and Technology of Advanced Materials **18**, 756 (2017).

[3] M. Rupp, A. Tkatchenko, K.-R. Müller, and O. A. von Lilienfeld, *Fast and Accurate Modeling of Molecular Atomization Energies with Machine Learning*, Phys. Rev. Lett. **108**, 058301 (2012).

[4] F. Faber, A. Lindmaa, O. A. von Lilienfeld, and R. Armiento, *Crystal Structure Representations for Machine Learning Models of Formation Energies*, Int. J. Quantum Chem. **115**, 1094 (2015).

[5] B. Ghosh et al., *Superior Performance of Silver Bismuth Iodide Photovoltaics Fabricated via Dynamic Hot-Casting Method under Ambient Conditions*, Adv. Energy Mater. **8**, 1802051 (2018).

[6] Y. Kim et al., *Pure Cubic-Phase Hybrid Iodobismuthates $AgBi_2I_7$ for Thin-Film Photovoltaics*, Angew. Chem. Int. Ed. **55**, 9586 (2016).

[7] I. Turkevych, S. Kazaoui, E. Ito, T. Urano, K. Yamada, H. Tomiyasu, H. Yamagishi, M. Kondo, and S. Aramaki, *Photovoltaic Rudorffites: Lead-Free Silver Bismuth Halides Alternative to Hybrid Lead Halide Perovskites*, ChemSusChem **10**, 3754 (2017).

[8] L. F. Mashadieva, Z. S. Aliev, A. V. Shevelkov, and M. B. Babanly, *Experimental Investigation of the Ag–Bi–I Ternary System and Thermodynamic Properties of the Ternary Phases*, Journal of Alloys and Compounds **551**, 512 (2013).

[9] H. C. Sansom et al., *$AgBiI_4$ as a Lead-Free Solar Absorber with Potential Application in Photovoltaics*, Chem. Mater. **29**, 1538 (2017).

[10] M. Nishiwaki and H. Fujiwara, *Highly Accurate Prediction of Material Optical Properties Based on Density Functional Theory*, Computational Materials Science **172**, 109315 (2020).

[11] O.S. Center, *Ohio Supercomputer Center*, (1987).